ACS OMEGA

Article

http://pubs.acs.org/journal/acsodf

Sea Urchin Spicule Matrix Proteins Form Mesoscale "Smart" Hydrogels That Exhibit Selective Ion Interactions

Martin Pendola, Anastasia Davidyants, Yong Seob Jung, and John Spencer Evans*

Center for Skeletal Biology and Craniofacial Medicine, Laboratory for Chemical Physics, New York University College of Dentistry, 345 East 24th Street, New York, New York 10010, United States

Supporting Information

ABSTRACT: In the sea urchin embryo spicule, there exists a proteome of >200 proteins that are responsible for controlling the mineralization of the spicule and the formation of a fracture-resistant composite. In this report, using recombinant proteins, we identify that two protein components of the spicule, SM30B/C and SM50, are hydrogelators. Because of the presence of intrinsic disorder and aggregation-prone regions, these proteins assemble to form porous mesoscale hydrogel particles in solution. These hydrogel particles change their size, organization, and internal structure in response to pH and ions, particularly Ca(II), which indicates that these behave as ion-responsive or "smart" hydrogels. Using diffusion-ordered spectroscopy NMR, we find that both hydrogels affect the diffusion of water, but only SM50 affects the diffusion of an anionic solute. Thus, the extracellular matrix of the spicule consists of several hydrogelator proteins which are responsive to solution conditions and can control the diffusion of water and solutes, and these proteins will serve as a model system for designing ion-responsive, composite, and smart hydrogels.

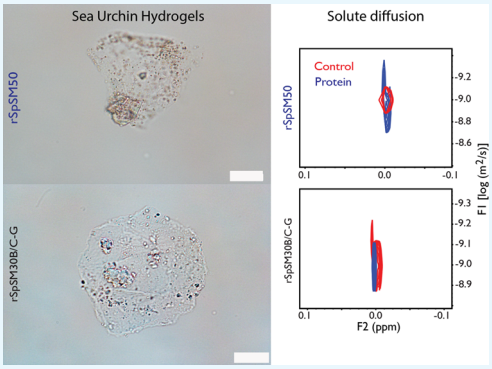

INTRODUCTION

Rapid developments have occurred in hydrogel technology, spanning such applications as drug delivery, adhesion, nanoparticle organization, cell culture, and so on.[1−6] Hydrogels are essentially highly hydrated polymer networks possessing bonding or nonbonding interchain interactions. Hydrogel properties, such as diffusion, internal transport, and mechanical strength, are directly linked to the degree of swelling and the chemistries offered by the polymer network itself.[1−7] At present, there are two areas of hydrogel research that have garnered attention. The first is "smart" hydrogel technology involving the creation of polymer networks capable of responding to multiple environmental triggers, such as pH or temperature.[1,2,4,6,7] The second is "composite" hydrogels, where small inorganic particles become incorporated into the gel network and enhance the mechanical properties of the gel phase.[3,5] If we can gain further insights into engineering improvements in these areas, then the hydrogel technology and its corresponding applications will advance more rapidly.

Notably, our ability to jumpstart existing technologies can be enhanced by the study of organisms in nature. Although synthetic polymer networks are commonly used for hydrogel generation,[1−7] there are natural polymeric systems that also lend themselves to hydrogel formation, such as collagen, chitosan, fibrin, agarose, hyaluronic acid, and cellulose.[2] Interestingly, there are some extracellular matrices (ECMs) in nature that may offer bioinspired insights into hydrogel technologies. One of these is sea urchin skeletal elements: protective embryonic spicules and adult spines, where ECM proteins combine to form an environment for inorganic nanoparticle nucleation (calcium carbonates), assembly, and the creation of a fracture-resistant inorganic−organic composite.[8−11] This protein system may play an important role in creating a meshwork within the ECM that limits ion diffusion and creates ultrasmall volume compartmentalization that controls the mineral nucleation process.[8−11]

There are more than 200 different proteins[8−18] that comprise the embryonic spicule matrix, and several proteins have been identified as regulators of the spicule mineralization process.[8−18] Many of these proteins have very interesting properties, such as the presence of intrinsic disorder or unfolded structure and amyloid-like cross-beta strand aggregation-prone sequences, both of which promote protein−protein aggregation and assembly.[17,18] This assembly process creates supramolecular complexes or protein aggregates that are hydrogel-like in appearance[17,18] and possess a particle and filmlike character on surfaces. These protein hydrogels have been demonstrated to control early stages of mineralization[17,18] and to modify the surfaces and interiors of existing crystals.[17,18] However, the physical nature of these protein hydrogels has not been fully explored: do these smart hydrogels respond to environmental changes, and if so, do they possess any interesting properties that might advance our understanding and development of synthetic hydrogels?

Received: June 2, 2017
Accepted: September 13, 2017
Published: September 26, 2017

DOI: 10.1021/acsomega.7b00719
ACS Omega 2017, 2, 6151−6158

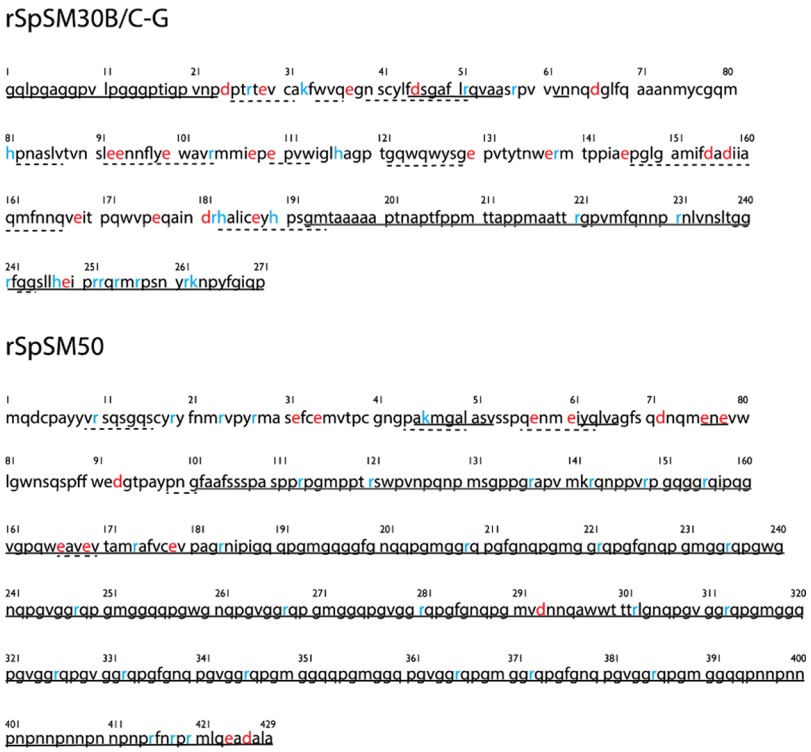

Figure 1. Primary sequence and bioinformatics analysis of the mature, processed SpSM30B/C and SpSM50 proteins (UniProtKB accession numbers P28163 and P11994, respectively).[8−11] Predicted regions of intrinsic disorder sequence regions (solid lines using DISOPRED[33] and IUP[34] algorithms) and cross-beta strand sequence regions (dashed lines using AGGRESCAN,[35] TANGO,[36] and ZIPPER_DB.[37]). Negative (red) and positive (blue) charged amino acids are indicated.

In this article, we examine two intrinsically disordered, aggregation-prone embryonic spicule matrix proteins (Figure 1): the glycoprotein SpSM30B/C [isoelectric point (pI) = 5.73, 270 AA, molecular weight (MW) = 33 287.4 Da *Strongylocentrotus purpuratus*] and SpSM50 (pI = 10.7, 428 AA, MW = 44 541 Da),[8−11,17,18] of which SpSM50 is the nonglycosylated major protein component of the spicule matrix. Both proteins are nonphosphorylated, distinctly different in net charge, and possess intrinsically disordered and amyloid-like cross-beta strand aggregation sequences (Figure 1).[17,18] Each protein forms mesoscale protein hydrogel particles that modify crystal growth directions,[17] introduce surface nanotexturing and subsurface porosities to growing calcium carbonate crystals, promote faceted crystal growth, and capture and organize mineral nanoparticles.[17,18] Using a recombinant version of both proteins (insect cell-expressed, glycosylated rSpSM30B/C-G and bacterially expressed rSpSM50)[17,18] and biophysical techniques, we confirm that these spicule matrix proteins are in fact smart hydrogelators: they change their size, organization, and internal structure in response to pH, Na^+, and Ca^{2+}. Further, using ^{1}H PFG NMR, we confirm that both hydrogels affect the diffusion of water protons in similar ways but react differently to an anionic tracer molecule. Thus, the ECM of mineralized sea urchin spicules is a protein-based hydrogel. Further, recombinant proteins such as rSpSM30B/C-G and rSpSM50, alongside their nacre protein hydrogelator counterparts,[19−25] can serve as models for developing smart or responsive hydrogelation systems.

MATERIALS AND METHODS

Recombinant Synthesis, Purification, and Preparation of rSpSM30B/C-G and rSpSM50. The gene synthesis, cloning, bacterial expression, and purification of the insect cell-expressed recombinant glycoprotein rSpSM30B/C-G were performed by GenScript USA (Piscataway, NJ, USA; www.genscript.com/) using their proprietary OptimumGene system and baculovirus recombinant expression systems as described elsewhere.[17] The gene synthesis, cloning, bacterial expression, and purification of the recombinant rSpSM50 were performed by BiologicsCorp (Indianapolis, IN, USA) as described elsewhere.[18] For subsequent experimentation, both samples were created by exchanging and concentrating appropriate volumes of stock solution into 30 nm filtered Fisher AFM-grade water (Fisher Scientific, USA) or other appropriate buffers using Amicon Ultra 0.5, 3 kDa molecular weight cutoff (Millipore Corporation, USA). For the studies listed in this report, the following buffer conditions were utilized: 10 mM *N*-(2-hydroxyethyl)piperazine-*N*′-ethanesulfonic acid (HEPES), pH 8.0 (denoted as low ionic strength conditions); 8.9 mM NaH_2PO_4, pH 4.0; 10 mM HEPES/30 mM NaCl, pH 8.0; and 10 mM HEPES/10 mM $CaCl_2$, pH 8.0. All buffers were prepared in 30 nm filtered Fisher AFM water (Fisher Scientific, USA) and filtered at 0.2 μm after pH adjustment to purge particulates.

Light Microscopy Imaging of Protein Hydrogel Particles. For the detection of mesoscale protein hydrogel particles, 5 μL of 50 μM rSpSM30B/C-G and 10 μM rSpSM50 solutions in the appropriate buffer (see above) was placed on a clean glass slide with a glass coverslip and imaged using bright field microscopy (100× objective, Nikon DS-U3 light microscope). Note that because of the differences in aggregation propensity and hydrogelation, higher rSpSM30B/C-G protein concentrations were required to generate sufficiently large hydrogels for visualization purposes.[17−19,21,25]

DOI: 10.1021/acsomega.7b00719
ACS Omega 2017, 2, 6151−6158

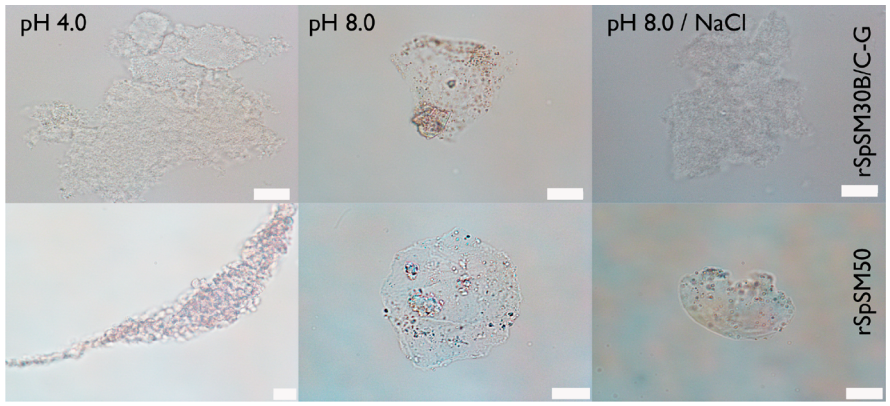

Figure 2. Light microscopy images of rSpSM protein hydrogel particles in 10 mM HEPES, pH 8.0; 10 mM HEPES/30 mM NaCl, pH 8.0; and 8.9 mM NaH_2PO_4, pH 4.0. Scale bars = 10 microns.

Flow Cytometry Experiments of Protein Aggregates. The aggregation of rSpSM30B/C-G and rSpSM50 (15 and 1.5 μM final concentrations, respectively) was studied in the above-mentioned buffers. Because of the strong aggregation propensities, lower concentrations of rSpSM50 were utilized to avoid precipitation issues. Samples were constituted and allowed to sit for 5 min prior to analysis. Aggregation measurements were performed using a multiparameter cell analyzer CytoFLEX (Beckman Coulter, CA, USA). Each sample solution (100 μL) was analyzed at a continuous flow rate of 10 μL/min using four laser excitation lines of 405, 488, 561, and 640 nm to register two light scattering parameters (forward-scattered component or FSC-A and side-scattered component or SSC-A; detailed definitions can be found in the legend of Figure 3)[25−28] and the number of events for each sample. Data were collected using the CytExpert 1.2.11.0 software designed for the instrument and processed using FlowJo software (Tree Star, OR, USA).

^{1}H NMR PFG DOSY Diffusion Experiments. To measure the interactions of solvent water and a traceable charged solute with the protein hydrogels, we performed ^{1}H NMR PFG experiments on the following samples (3 mm NMR tubes). A control sample consisted of 150 μL of 30 nm Fisher UltraPure water (Fisher Scientific, USA) containing 10% v/v 99.9% D_2O (Cambridge Scientific Labs, USA) and 133 μM 3-(trimethylsilyl)propionic-2,2,3,3-d_4 acid sodium salt (d_4-TSP) (Cambridge Isotope Labs, USA). The rSpSM30B/C-G and rSpSM50 samples consisted of 22 μM protein in 150 μL of 30 nm Fisher UltraPure water with 133 μM d_4-TSP. Each sample was titrated to pH 8.0 using microliter volumes of HCl or NaOH. ^{1}H NMR experiments were conducted at 25 °C on a Bruker AVANCE-700 NMR spectrometer using a 3 mm cryoprobehead. Diffusion experiments for all samples were performed at a field strength of 700 MHz using a two-dimensional (2D) diffusion-ordered spectroscopy (DOSY) experiment[29−32] for diffusion measurement using stimulated echo, LED diffusion pulse sequence, bipolar gradient pulses, two spoil gradients, and a DOSY linear ramp of 16 points, with delays at 10, 0.1, 0.005, and 0.0002 s. All NMR data were analyzed and plotted using TopSpin software (Bruker BioSpin, USA).

Bioinformatics. To determine the location of disordered sequence regions within the SpSM30B/C-G and SpSM50 sequences, we employed the DISOPRED3[33] and IUP_PRED[34] prediction algorithms using default parameters. Subsequently, we utilized TANGO,[35] AGGRESCAN,[36] and ZIPPER_DB[37] with default parameters to globally identify putative cross-beta strand sequence regions which exhibit association propensities (Figure 1).

RESULTS AND DISCUSSION

rSpSM Proteins Form Hydrogel-Like Particles That Respond to pH and Ionic Strength Conditions. Our initial reference point is pH 8.0, which mimics the pH utilized in our past in vitro mineralization studies of rSpSM50 and rSPSM30B/C-G.[17,18] Note that the pH of the embryonic spicule matrix is not known at present, so we must rely on the in vitro pH 8.0 as the mineralization standard[17,18] for the time being. As shown in Figure 2, light microscopy studies confirm that both rSpSM30B/C-G and rSpSM50 form translucent particles at pH 8.0 that appear gel-like. These particles have irregular morphologies and appear to be porous as evidenced by the presence of voidlike regions within the particles. For comparison, we studied these protein particles at 8.9 mM NaH_2PO_4, pH 4.0 and 10 mM HEPES/30 mM NaCl, pH 8.0, with both buffer conditions possessing the same ionic strength value as 10 mM $CaCl_2$/10 mM HEPES. As we shall see, similarities in ionic strength values allow cross comparisons between these conditions and latter Ca^{2+} studies.

We will first consider low pH conditions (pH 4.0) which are below the pI of both proteins. Note that in Figure 2 there are dimensional and morphological changes in mesoscale hydrogel particles in response to protein side-chain protonation. For rSpSM30B/C-G, a shift to lower pH results in the formation of larger hydrogels which consist of subassemblies, evidence of clustering, textured surfaces, and no observable large voids or porosities. A similar result is obtained for rSpSM50 but with a much more significant morphological shift to a sicklelike hydrogel consisting of multiple subassemblies. In both proteins, low pH conditions foster the formation of smaller hydrogel particles which then coassemble into larger hydrogels. However, slightly different results are obtained in pH 8.0/NaCl solutions, where small hydrogel particle coassemblies are noted for rSpSM30B/C-G but not for rSpSM50 (Figure 2). We attribute this difference to the fact that rSpSM30B/C-G is anionic at pH 8.0 (pI = 5.73) because of the presence of Asp, Glu, and sulfated/carboxylated oligosaccharide chains.[17] Thus, this protein would be more susceptible to electrostatic shielding or neutralization from Na^+ and Cl^- than rSpSM50 (pI = 10.7), which is cationic in nature because of the presence of 25 Arg groups.[18] This electrostatic susceptibility, in turn, would lead to

DOI: 10.1021/acsomega.7b00719
ACS Omega 2017, 2, 6151−6158

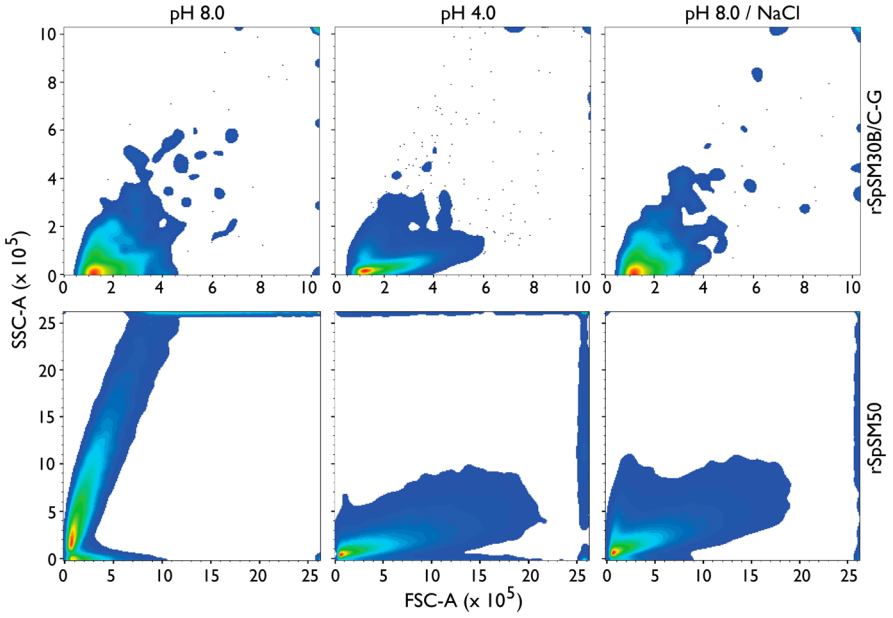

Figure 3. Flow cytometry 2D density plots (FSC vs SSC) of 15 μM rSpSM30B/C-G and 1.5 μM rSpSM50 proteins in 10 mM HEPES, pH 8.0; 10 mM HEPES/30 mM NaCl, pH 8.0; and 8.9 mM NaH_2PO_4, pH 4.0. FSC refers to a parameter measuring light scattered less than 10° as a particle passes through the laser beam and is related to the particle size. SSC is proportional to particle granularity or internal complexity and is a measurement of mostly refracted and reflected light that occurs at any interface within the particle where there is a change in RI. SSC is collected at approximately 90° to the laser beam by a collection lens and then redirected by a beam splitter to the appropriate detector.

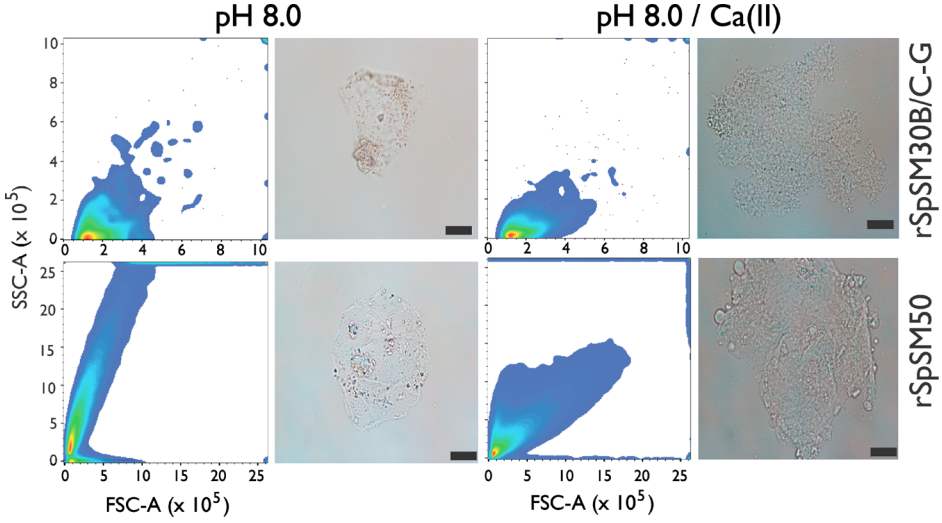

Figure 4. Light microscopy and 2D flow cytometry density plots for 15 μM rSpSM30B/C-G and 1.5 μM rSpSM50 in the presence and absence of 10 mM $CaCl_2$ in 10 mM HEPES, pH 8.0.

NaCl-induced changes in hydrogel particle aggregation for anionic rSpSM30B/C-G but not for cationic rSpSM50.[17,18]

rSpSM Hydrogel Particles in Flow Exhibit Particle Size and Internal Granularity Changes in Response to pH and Ionic Strength. To confirm the external and internal changes that occur with mesoscale rSpSM hydrogel particles as a function of buffer conditions, we applied a technique, flow cytometry, typically used for analyzing transparent micron-sized cell populations[25−28] to map physical changes in translucent mesoscale protein particles under buffer conditions that are parallel to our light microscopy studies (Figure 3). There are two light scattering parameters that one can monitor for particles under constant flow: (1) FSC (x-axis) to determine particle size distribution and (2) SSC (y-axis) to measure refracted and reflected light that occurs at any interface within the particles where there is a change in refractive index (RI) that results from variations in particle granularity or internal structure.[25−28] Note that our flow cytometry experiments do not provide exact particle size data but only the distributions of particle sizes.

As we observe in Figure 3, low ionic strength conditions at pH 8.0 generate a distribution of hydrogel particle sizes and internal structure or granularities for both proteins, with the evidence of ∼20 different populations for rSpSM30B/C-G and a single, heterogeneous population for rSpSM50. When the transition drops to pH 4.0, the size distributions and the internal structure shift to smaller values for both the proteins, with the number of distinct rSpSM30B/C-G hydrogel particle

DOI: 10.1021/acsomega.7b00719
ACS Omega 2017, 2, 6151−6158

Table 1. ^{1}H NMR DOSY—Determined Diffusion Coefficient [(D) 25 °C, (m^2/s)]

species	(−)rSpSM30	(+)rSpSM30	(−)rSpSM50	(+)rSpSM50
water	5.337×10^{-10}	3.236×10^{-9}	5.337×10^{-10}	3.164×10^{-9}
TSP	9.977×10^{-10}	1.004×10^{-9}	9.968×10^{-10}	4.203×10^{-10}

populations decreasing by 50%. This suggests that the protonation of anionic groups, particularly in rSpSM30B/C-G, leads to changes in the aggregate structure and dimension, which we observed in the light microscope (Figure 2). To some extent the same phenomenon is observed in the presence of NaCl (Figure 3), where relative to low ionic strength conditions at pH 8.0 we see a decrease in both FSC and SSC parameters, indicating that ion pairing of Na^+ and Cl^- ions with anionic and cationic charged groups, respectively, on both proteins leads to dimensional and internal structural changes, again in agreement with our light microscopy data (Figure 2).

Response of rSpSM Hydrogels to Ca^{2+}. To determine how rSpSM hydrogel particles would respond to a mineralization-like environment,[17,18] we next compared the morphology, particle size distribution, and particle granularity of each rSpSM protein hydrogel particle in the presence and absence of 10 mM $CaCl_2$ at pH 8.0 in 10 mM HEPES (Figure 4), which mimics the conditions utilized in previous in vitro mineralization assays.[17,18] An examination of the light microscopy images of both proteins reveals an increase in hydrogel particle size. Further, in the case of rSpSM30B/C-G, the hydrogels appear to consist of multiple hydrogel subunit particles, as we witnessed in the pH 4.0 and pH 8.0/NaCl scenarios (Figure 2). However, in the case of rSpSM50, we observe a different effect of Ca^{2+} on hydrogel particle morphology: the presence of exterior blebs, which may be indicative of a continuing assembly process involving smaller hydrogel subunits (Figure 4). These results are supported by our flow cytometry dataset, which show that both proteins experience an increase in particle size distributions in the presence of Ca(II) (i.e., increase in the FSC-A component, Figure 4). Interestingly, the particle granularity or the internal structure of the hydrogel particles appears to decrease in the presence of Ca(II), which may reflect changes due to the particle composition (e.g., shift to multiple subunit components and interfaces and changes in the internal porosities). Again, as described for the pH 4.0 and NaCl conditions, these changes reflect charge-shielding effects that protons, counterions, and Ca(II) ions exert on both protein hydrogels. Overall (Figures 2−4), we conclude that the recombinant spicule matrix proteins rSpSM30B/C-G and rSpSM50 are hydrogelators that form smart ion-responsive mesoscale gel particles in solution, like what we have noted for mollusk shell nacre proteins.[21,25]

rSpSM Hydrogel Particles Affect Tracer and Water Diffusion. In earlier studies, we determined that rSpSM30B/C-G and rSpSM50 affected the kinetics of prenucleation clusters (PNCs), an early intermediate that assembles to form amorphous calcium carbonate (ACC).[17,18] ACC is an important intermediate in spiculogenesis and eventually transforms into a single-crystal calcite.[12−14] Interestingly, we found that rSpSM30B/C-G stabilized ACC, whereas rSpSM50 destabilized ACC in vitro. Hypothetically, protein hydrogels could contribute to these phenomena via changes in ion cluster associations and ion kinetics, either via surface or internal interactions with cations and anions or mediating the release of water from the clusters.[37,38] Moreover, both protein hydrogels are noted to possess mineral nanoparticles within their matrices,[17,18] which suggest that the hydrated ionic clusters appear within the hydrogels during the nucleation process.

Thus, to explain these in vitro phenomena, we need to determine whether rSpSM hydrogel particles are solvent- and solute-interactive. To achieve this, we applied ^{1}H 2D PFG diffusion experiments (DOSY)[29−32] to probe the effect of both protein hydrogel particles on bulk water protons (Table 1; Figure S1, Supporting Information) and on a small, traceable anionic solute, d_4-TSP, which serves both as a carbonate/bicarbonate surrogate and a ^{1}H chemical shift reference (Figure 5). In the DOSY experiment, water and TSP molecules become

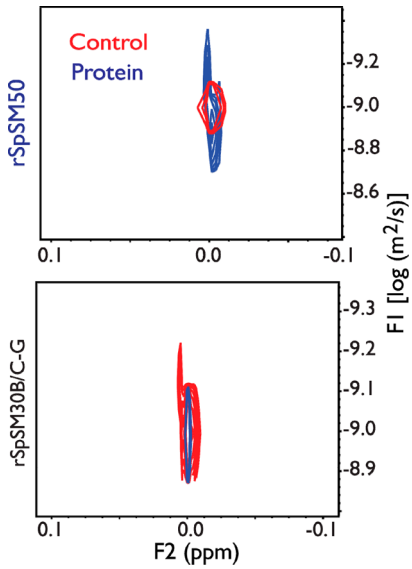

Figure 5. Overlay of 700 MHz ^{1}H 2D DOSY PFG diffusion experiments of 90% 30 nm filtered H_2O/10% 99.9% D_2O/133 μM d_4-TSP sample in the presence (blue) and absence (red) of 22 μM rSpSM30B/C-G and rSpSM50, 150 μL volume. The log of the diffusion coefficient is plotted on the y-axis (F1 domain) and determined from the contour plot maxima for each sample.

spatially labeled based on their position in the NMR tube. If these molecules move after the encoding, or "labeling", period during the diffusion time (Δ) that follows in the pulse sequence, then their new position can be decoded with a second gradient (F1 axis) and a temperature-dependent diffusion coefficient can be calculated.[29−32] Thus, any TSP or water molecules which interact with either hydrogel particle ensemble should exhibit a noticeable change in their diffusion coefficients relative to species in the bulk state (i.e., in the absence of protein). Three caveats should be mentioned: (1) We presume that the large, denser hydrogel particles (Figures 3 and 4) have settled out to the bottom of the tube during the NMR experiments; however, there may be some population of hydrogel particles whose sizes and densities allow them to remain suspended in the solution rather than settle out. Unfortunately, for either protein, we do not know the percentage of hydrogel particles that are suspended or settled out in solution, and thus, we assume that the dataset reflects both hydrogel states and their averaged effects on TSP

DOI: 10.1021/acsomega.7b00719
ACS Omega 2017, 2, 6151−6158

diffusion. (2) We assume that the interactions of the hydrogels with TSP and water reflect an averaging of internal and external hydrogel surface interactions with either species, in which unfortunately our NMR experiments are unable to resolve as separate phenomena. (3) Because DOSY experiments are optimized for isotropic species,[29−32] any species that is bound tightly to hydrogel particles becomes anisotropic and thus cannot be detected by these experiments because of their inhomogeneous broadening effects. Thus, the DOSY experiments primarily measure the effect of each hydrogel on the diffusion of bulk solution species.

Using parallel protein-free and protein-containing samples, we detected nearly identical perturbations of bulk water diffusion by both proteins relative to the bulk protein-free state at 25 °C (Table 1; Supporting Information, Figure S1): an increase in water proton diffusion by a factor of ∼7×. It is known that hydrogels attract water avidly,[1−7,37,38] and our DOSY results indicate that both protein hydrogels attract or exchange protons with the bulk water phase over the course of the NMR experiment to a similar degree, thus increasing the observed water diffusion during this period. By contrast, different results were obtained for TSP (Figure 5, Table 1), which exists in a molar ratio of 6:1 relative to each protein. Here, the diffusion coefficients for TSP in the presence and absence of rSpSM30B/C are nearly identical, suggesting that the diffusion of the tracer is only minimally affected by this protein hydrogel. However, for rSpSM50, the diffusion of the TSP molecule is reduced by nearly a factor of 2 relative to the bulk state and to rSpSM30B/C-G. We attribute these differences in TSP diffusion to the fact that rSpSM30B/C-G is anionic and may be repulsive to the TSP sulfonate. Conversely, rSpSM50 has a pI of 10.7 and 25 Arg residues,[18] and thus, the cationic nature of this protein may attract the anionic TSP molecule to the hydrogel and thus restrict the diffusion of this tracer in bulk solution. Thus, rSpSM hydrogels affect the diffusion of bulk water in a similar fashion but differ in terms of the diffusion of the anionic tracer. This may help to explain why each protein affects the water- and ion-dependent ACC stabilization process[37,38] in different ways.

In summary, our study verifies that the recombinant versions of *S. purpuratus* sea urchin spicule matrix proteins SM50 and SM30B/C are hydrogelators (Figures 2−4), that is, both proteins form porous hydrogel particles in solution. Note that it remains to be seen whether hydrogelation also takes place in situ with the native versions of each protein, which may contain post-translational modifications yet to be discovered (e.g., phosphorylation).[10] The ability of both recombinant proteins to form hydrogels lies in two common sequence traits (Figure 1):[17,18] (a) intrinsic disorder, where the lack of folded structure introduces conformational instability and thus protein molecules become interactive with one another (i.e., aggregation) to achieve internal stabilization;[17,18,32,33] and (b) amyloid-like cross-beta strand aggregation domains, which also induce protein−protein aggregation.[17,18,34−36] We note that other invertebrate skeletal systems, specifically the mollusk nacre layer, also possess hydrogelator proteins with qualitatively similar sequence traits.[21−25] This suggests that protein disorder and aggregation propensities play an important role in the protein hydrogel-mediated biomineralization process within sea urchins and mollusks.

The discovery of porous spicule matrix protein hydrogels represents a step forward in our understanding of the biomineralization process in the sea urchin spicule. As summarized elsewhere,[1−7,21,25] porous hydrogels provide several key features for the nucleation process and crystal assembly: volume confinement, compartmentalization, nanoparticle assembly, and organization. Given that SpSM50 and SpSM30 are among the most abundant proteins in the spicule matrix during spiculogenesis,[9−11,15,16] we would argue that the spicule matrix possesses a hydrogel environment within which nucleation, nanoparticle assembly, ACC formation, and ACC-to-calcite transformation take place. We note that the mollusk shell nacre layer also possesses a protein-based hydrogel environment,[19−25] and thus, both mineralized skeletal tissues may use similar molecular strategies in constructing fracture-resistant biocomposites.

The intriguing response of the protein hydrogel particles to different ionic conditions (Figures 2−4) indicates that the rSpSM protein hydrogel particles are ion-responsive or smart,[1−7] that is, their morphologies, particle size distributions, and internal structures respond to changes in protonation or ions. Perhaps the most dramatic changes were noted at low pH, particularly for rSpSM50 hydrogels, where a multi-subunit extended morphology formed (Figure 2). This suggests that Asp, Glu, and carboxylate side chains (and in the case of rSpSM30B/C-G, sulfated, carboxylated oligosaccharide chains) play an important role in SpSM hydrogelation under different conditions. We believe that ion responsiveness may serve as a "trigger"[1−7] for hydrogel participation in $CaCO_3$ nucleation events, that is, hydrogels change size, morphology, and internal structure in response to Ca(II) ions (Figure 4), which in turn can affect the assembly and organization of mineral nanoparticles,[17,18] an important event in the crystallization by the particle attachment[41,42] mechanism that ultimately leads to a single-crystal calcite formation in the forming spicule.[12]

Our study also sheds light on the ability of biomineral-associated protein hydrogels to interact with bulk water and charged solutes (Figure 5, Table 1; Figure S1, Supporting Information). Here, both hydrogels increase the diffusion of water protons over time, but only cationic rSpSM50 exhibits perturbation of anionic TSP diffusion over time. Recent studies revealed that hydration of ion clusters and ACC is highly important to the calcium carbonate mineralization process, in that water network dynamics play a role in phase separation during nucleation.[39] Further, ion clustering involves water release from the ion hydration layers and is believed to accompany PNC formation during nucleation.[40] Thus, protein hydrogels could play an important role in these processes by mediating water release or diffusion from ion clusters.[39,40,43−46] Further, the anionic and cationic nature of SpSM30B/C-G and rSpSM50 hydrogels, respectively, may differentially influence the movement and availability of hydrated ionic species (Figure 5) such as carbonate, bicarbonate, and PNCs[43−46] during nucleation and may be the basis for why each protein affects ACC stabilization in different ways.[17,18] Obviously, additional experimentation will be required to determine how each protein hydrogel affects ion cluster mobility, hydration, and assembly to further establish this possibility.

Finally, what insights do spicule matrix protein hydrogels offer materials science and nanotechnology? As we stated earlier for nacre proteins,[25] we believe that there are several important lessons that one can glean from this sea urchin study. The first is that charged, disordered, aggregation-prone polymers can form ion-responsive hydrogels in solution under a wide variety of conditions (Figures 2−4). The second is that the predominance of either anionic or cationic charged

DOI: 10.1021/acsomega.7b00719
ACS Omega 2017, 2, 6151−6158

groups may allow for variations in hydrogel morphology and internal structure (Figures 2−4) and the response of charged solutes to the hydrogel (Figure 5, Table 1). Finally, considering our light microscopy and flow cytometry observations (Figures 2−4), we speculate that the changes in particle granularity or internal RI reflect changes in hydrogel porosities, either in terms of the number of porosities, their size, and/or their location within the protein hydrogel particles.[17,18,25] In turn, these adjustments to ionic media may eventually influence the formation, size, and distribution of mineral nanoparticles within the hydrogels.[17,18] Thus, similar to their nacre counterparts,[19−25] spicule matrix protein hydrogels are worthy of further exploration in future studies, such that we can apply these concepts to new and useful composite, responsive smart hydrogels for materials and nanotechnology applications.[1−7]

■ ASSOCIATED CONTENT

Supporting Information

The Supporting Information is available free of charge on the ACS Publications website at DOI: 10.1021/acsomega.7b00719.

^{1}H NMR 2D DOSY water spectra of protein-free (control) and rSpSM30B/C-G and rSpSM50 samples (PDF)

■ AUTHOR INFORMATION

Corresponding Author

*E-mail: jse1@nyu.edu (J.S.E.).

ORCID

John Spencer Evans: 0000-0002-9565-7296

Author Contributions

All authors have given approval to the final version of the manuscript.

Funding

This research was supported by the Life Sciences Division, U.S. Army Research Office, under award W911NF-16-1-0262 (J.S.E.).

Notes

The authors declare no competing financial interest.

■ ACKNOWLEDGMENTS

This report represents contribution number 88 from the Laboratory for Chemical Physics, New York University.

■ ABBREVIATIONS

SpSM, *S. purpuratus* spicule matrix proteins; rSpSM30B/C-G, insect cell-expressed recombinant *S. purpuratus* spicule matrix protein SM30, hybrid isoform B/C, glycosylated; rSpSM50, bacterial-expressed recombinant *S. purpuratus* spicule matrix protein SM50; ACC, amorphous calcium carbonate; PNC, prenucleation cluster; FSC, forward-scattered component; SSC, side-scattered component; DOSY, diffusion-ordered spectroscopy; d_4-TSP, deuterated 3-(trimethylsilyl)propionic-2,2,3,3-d_4 acid sodium salt; ECM, extracellular matrix

■ REFERENCES

(1) Samchenko, Y.; Ulberg, Z.; Korotych, O. Multipurpose smart hydrogel systems. *Adv. Colloid Interface Sci.* **2011**, *168*, 247−262.

(2) Buwalda, S. J.; Boere, K. W. M.; Dijkstra, P. J.; Feijen, J.; Vermonden, T.; Hennink, W. E. Hydrogels in a historical perspective: From simple networks to smart materials. *J. Controlled Release* **2014**, *190*, 254.

(3) Gao, W.; Zhang, Y.; Zhang, Q.; Zhang, L. Nanoparticle-hydrogel: A hybrid biomaterial system for localized drug delivery. *Ann. Biomed. Eng.* **2016**, *44*, 2049−2061.

(4) Du, X.; Zhou, J.; Shi, J.; Xu, B. Supramolecular hydrogelators and hydrogels: From soft matter to molecular biomaterials. *Chem. Rev.* **2015**, *115*, 13165−13307.

(5) Thoniyot, P.; Tan, M. J.; Karim, A. A.; Young, D. J.; Loh, X. J. Nanoparticle-hydrogel composites: Concept, design, and applications of these promising, multi-functional materials. *Adv. Sci.* **2015**, *2*, 1400010.

(6) Xia, L.-W.; Xie, R.; Ju, X.-J.; Wang, W.; Chen, Q.; Chu, L.-Y. Nano-structured smart hydrogels with rapid response and high elasticity. *Nat. Commun.* **2013**, *4*, 2226.

(7) Lim, H. L.; Hwang, Y.; Kar, M.; Varghese, S. Smart hydrogels as functional biomimetic systems. *Biomater. Sci.* **2014**, *2*, 603−618.

(8) Cameron, R. A.; Samanta, M.; Yuan, A.; He, D.; Davidson, E. SpBase: the sea urchin genome database and web site. *Nucleic Acids Res.* **2009**, *37*, D750−D754. . http://www.spbase.org/

(9) Sea urchin genome sequencing consortium.; et al. The genome of the sea urchin Strongylocentrotus purpuratus. *Science* **2006**, *314*, 941−952.

(10) Mann, K.; Poustka, A. J.; Mann, M. The sea urchin (Strongylocentrotus purpuratus) test and spine proteomes. *Proteome Sci.* **2008**, *6*, 22.

(11) Mann, K.; Wilt, F. H.; Poustka, A. J. Proteomic analysis of sea urchin (Strongylocentrotus purpuratus) spicule matrix. *Proteome Sci.* **2010**, *8*, 33.

(12) Seto, J.; Ma, Y.; Davis, S. A.; Meldrum, F.; Gourrier, A.; Kim, Y.-Y.; Schilde, U.; Sztucki, M.; Burghammer, M.; Maltsev, S.; Jäger, C.; Cölfen, H. Structure-property relationships of a biological mesocrystal in the adult sea urchin spine. *Proc. Natl. Acad. Sci. U.S.A.* **2012**, *109*, 3699−3704.

(13) Berman, A.; Addadi, L.; Kvick, A.; Leiserowitz, L.; Nelson, M.; Weiner, S. Intercalation of sea urchin proteins in calcite: Study of a crystalline composite material. *Science* **1990**, *250*, 664−667.

(14) Aizenberg, J.; Hanson, J.; Koetzle, T. F.; Weiner, S.; Addadi, L. Control of macromolecule distribution within synthetic and biogenic single calcite crystals. *J. Am. Chem. Soc.* **1997**, *119*, 881−886.

(15) Livingston, B. T.; Killian, C. E.; Wilt, F.; Cameron, A.; Landrum, M. J.; Ermolaeva, O.; Sapojnikov, V.; Maglott, D. R.; Buchanan, A. M.; Ettensohn, C. A. A Genome-wide analysis of biomineralization-related proteins in the sea urchin Strongylocentrotus purpuratus. *Dev. Biol.* **2006**, *300*, 335−348.

(16) Wilt, F.; Croker, L.; Killian, C. E.; McDonald, K. Role of LSM34/SpSM50 proteins in endoskeletal spicule formation in sea urchin embryos. *Invertebr. Biol.* **2008**, *127*, 452−459.

(17) Jain, G.; Pendola, M.; Rao, A.; Cölfen, H.; Evans, J. S. A model sea urchin spicule matrix protein self-associates to form mineral-modifying protein hydrogels. *Biochemistry* **2016**, *55*, 4410−4421.

(18) Jain, G.; Pendola, M.; Huang, Y.-C.; Gebauer, D.; Evans, J. S. A model sea urchin spicule matrix protein, rSpSM50, is a hydrogelator that modifies and organizes the mineralization process. *Biochemistry* **2017**, *56*, 2663−2675.

(19) Chang, E. P.; Evans, J. S. Pif97, a von Willebrand and Peritrophin biomineralization protein, organizes mineral nanoparticles and creates intracrystalline nanochambers. *Biochemistry* **2015**, *54*, 5348−5355.

(20) Perovic, I.; Chang, E. P.; Lui, M.; Rao, A.; Cölfen, H.; Evans, J. S. A nacre protein, n 16.3, self-assembles to form protein oligomers that participate in the post-nucleation spatial organization of mineral deposits. *Biochemistry* **2014**, *53*, 2739−2748.

(21) Pendola, M.; Jain, G.; Davidyants, A.; Huang, Y.-C.; Gebauer, D.; Evans, J. S. A nacre protein forms mesoscale hydrogels that "hijack" the biomineralization process within a seawater environment. *CrystEngComm* **2016**, *18*, 7675−7679.

(22) Perovic, I.; Verch, A.; Chang, E. P.; Rao, A.; Cölfen, H.; Kröger, R.; Evans, J. S. An oligomeric C-RING nacre protein influences prenucleation events and organizes mineral nanoparticles. *Biochemistry* **2014**, *53*, 7259−7268.

DOI: 10.1021/acsomega.7b00719
ACS Omega 2017, 2, 6151−6158

(23) Chang, E. P.; Russ, J. A.; Verch, A.; Kröger, R.; Estroff, L. A.; Evans, J. S. The Intrinsically Disordered C-RING Biomineralization Protein, AP7, Creates Protein Phases That Introduce Nanopatterning and Nanoporosities into Mineral Crystals. *Biochemistry* **2014**, *53*, 4317−4319.
(24) Chang, E. P.; Russ, J. A.; Verch, A.; Kröger, R.; Estroff, L. A.; Evans, J. S. Engineering of crystal surfaces and subsurfaces by framework biomineralization protein phases. *CrystEngComm* **2014**, *16*, 7406−7409.
(25) Perovic, I.; Davidyants, A.; Evans, J. S. Aragonite-associated mollusk shell protein aggregates to form mesoscale "smart" hydrogels. *ACS Omega* **2016**, *1*, 886−893.
(26) Hyka, P.; Lickova, S.; Přibyl, P.; Melzoch, K.; Kovar, K. Flow cytometry for the development of biotechnological processes with microalgae. *Biotechnol. Adv.* **2013**, *31*, 2−16.
(27) Cho, S. H.; Godin, J. M.; Chen, C.-H.; Qiao, W.; Lee, H.; Lo, Y.-H. Review Article: Recent advancements in optofluidic flow cytometer. *Biomicrofluidics* **2010**, *4*, 043001.
(28) Henel, G.; Schmitz, J. Basic theory and clinical applications of flow cytometry. *Lab. Med.* **2007**, *38*, 428−436.
(29) Morris, F. K.; Johnson, C. S. Resolution of discrete and continuous molecular size distributions by means of diffusion-ordered 2D NMR spectroscopy. *J. Am. Chem. Soc.* **1993**, *115*, 4291−4299.
(30) Johnson, C. S. Diffusion ordered nuclear magnetic resonance spectroscopy: principles and applications. *Prog. Nucl. Magn. Reson. Spectrosc.* **1999**, *34*, 203−256.
(31) Floquet, S.; Brun, S.; Lemonnier, J.-F.; Henry, M.; Delsuc, M.-A.; Prigent, Y.; Cadot, E.; Taulelle, F. Molecular weights of cyclic and hollow clusters measured by DOSY NMR spectroscopy. *J. Am. Chem. Soc.* **2009**, *131*, 17254−17259.
(32) Kagan, G.; Li, W.; Hopson, R.; Williard, P. G. Internally referenced diffusion coefficient−formula weight (D-FW) analysis of 31P diffusion-ordered NMR spectroscopy (DOSY). *Org. Lett.* **2009**, *11*, 4818−4821. Jones, D. T.; Cozzetto, D. DISOPRED3: precise disordered region predictions with annotated protein-binding activity. *Bioinformatics* **2014**, *31*, 857−863.
(33) Dosztányi, Z.; Csizmok, V.; Tompa, P.; Simon, I. IUPred: web server for the prediction of intrinsically unstructured regions of proteins based on estimated energy content. *Bioinformatics* **2005**, *21*, 3433−3434.
(34) Linding, R.; Schymkowitz, J.; Rousseau, F.; Diella, F.; Serrano, L. A comparative study of the relationship between protein structure and β-aggregation in globular and intrinsically disordered proteins. *J. Mol. Biol.* **2004**, *342*, 345−353.
(35) Conchillo-Solé, O.; de Groot, N. S.; Avilés, F. X.; Vendrell, J.; Daura, X.; Ventura, S. AGGRESCAN: a server for the prediction and evaluation of "hot spots" of aggregation in polypeptides. *BMC Bioinf.* **2007**, *8*, 65.
(36) Thompson, M. J.; Sievers, S. A.; Karanicolas, J.; Ivanova, M. I.; Baker, D.; Eisenberg, D. The 3D profile method for identifying fibril-forming segments of proteins. *Proc. Natl. Acad. Sci. U.S.A.* **2006**, *103*, 4074−4078.
(37) Xia, L.-W.; Xie, R.; Ju, X.-J.; Wang, W.; Chen, Q.; Chu, L.-Y. Nano-structured smart hydrogels with rapid response and high elasticity. *Nat. Commun.* **2013**, *4*, 2226.
(38) Lim, H. L.; Hwang, Y.; Kar, M.; Varghese, S. Smart hydrogels as functional biomimetic systems. *Biomater. Sci.* **2014**, *2*, 603−618.
(39) Sebastiani, F.; Wolf, S. L. P.; Born, B.; Luong, T. Q.; Cölfen, H.; Gebauer, D.; Havenith, M. Water dynamics from THz spectroscopy reveal the locus of a liquid-liquid binodal limit in aqueous $CaCO_3$ solutions. *Angew. Chem., Int. Ed.* **2017**, *56*, 490−495.
(40) Kellermeier, M.; Raiteri, P.; Berg, J. K.; Kempter, A.; Gale, J. D.; Gebauer, D. Entropy drives calcium carbonate ion association. *ChemPhysChem* **2016**, *17*, 3535−3541.
(41) De Yoreo, J. J.; Gilbert, P. U. P. A.; Sommerdijk, N. A. J. M.; Penn, R. L.; Whitelam, S.; Joester, D.; Zhang, H.; Rimer, J. D.; Navrotsky, A.; Banfield, J. F.; Wallace, A. F.; Michel, F. M.; Meldrum, F. C.; Cölfen, H.; Dove, P. M. Crystallization by particle attachment in synthetic, biogenic, and geologic environments. *Science* **2015**, *349*, aaa6760.
(42) Wallace, A. F.; Hedges, L. O.; Fernandez-Martinez, A.; Raiteri, P.; Gale, J. D.; Waychunas, G. A.; Whitelam, S.; Banfield, J. F.; De Yoreo, J. J. Microscopic Evidence for Liquid-Liquid Separation in Supersaturated $CaCO_3$ Solutions. *Science* **2013**, *341*, 885−889.
(43) Gebauer, D.; Kellermeier, M.; Gale, J. D.; Bergström, L.; Cölfen, H. Pre-nucleation clusters as solute precursors in crystallisation. *Chem. Soc. Rev.* **2014**, *43*, 2348−2371.
(44) Gebauer, D.; Volkel, A.; Cölfen, H. Stable prenucleation calcium carbonate clusters. *Science* **2008**, *322*, 1819−1822.
(45) Gebauer, D.; Cölfen, H. Prenucleation clusters and non-classical nucleation. *Nano Today* **2011**, *6*, 564−584.
(46) Demichelis, R.; Raiteri, P.; Gale, J. D.; Quigley, D.; Gebauer, D. Stable prenucleation mineral clusters are liquid-like ionic polymers. *Nat. Commun.* **2011**, *2*, 590.

DOI: 10.1021/acsomega.7b00719
ACS Omega 2017, 2, 6151−6158